Title: Thin Sea-ice Thickness as inferred from Passive Microwave and In Situ Observations

Authors: Kazuhiro Naoki[1], Jinro Ukita[1], Fumihiko Nishio[1,2], Masashige Nakayama[3], Josefino C. Comiso[4], and Al Gasiewski[5]

[1] *Graduate School of Science and Technology, Chiba University, Chiba, Japan*
[2] *Center for Environmental Remote Sensing, Chiba University, Chiba, Japan*
[3] *Kushiro Children's Museum, Hokkaido, Japan*
[4] *NASA Goddard Space Flight Center, Maryland, USA*
[5] *NOAA Earth System Research Laboratory, Colorado, USA*

Journal: JGR-Ocean for the special issue on "Large Scale Characteristics of the Sea Ice Cover from AMSR-E and other Satellite Sensors."

Abstract:

Since microwave radiometric signals from sea-ice strongly reflect physical conditions of a layer near the ice surface, a relationship of brightness temperature with thickness is possible especially during the early stages of ice growth. Sea ice is most saline during formation stage and as the salinity decreases with time while at the same time the thickness of the sea ice increases, a corresponding change in the dielectric properties and hence the brightness temperature may occur. This study examines the extent to which the relationships of thickness with brightness temperature (and with emissivity) hold for thin sea-ice, approximately <0.2 -0.3 m, using near concurrent measurements of sea-ice thickness in the Sea of Okhotsk from a ship and passive microwave brightness temperature data from an over-flying aircraft. The results show that the brightness temperature and emissivity increase with ice thickness for the frequency range of 10-37 GHz. The relationship is more pronounced at lower frequencies and at the horizontal polarization. We also established an empirical relationship between ice thickness and salinity in the layer near the ice surface from a field experiment, which qualitatively support the idea that changes in the near-surface brine characteristics contribute to the observed thickness-brightness temperature/emissivity relationship. Our results suggest that for thin ice, passive microwave radiometric signals contain, ice thickness information which can be utilized in polar process studies.

Popular Summary:

Other studies have shown that the extent and area of the Okhotsk Sea ice cover have been declining by about 9 % and 12 % per decade, respectively. To do mass balance and heat flux studies in the region, we need to know how the thickness distribution has been changing as well but continuous monitoring of ice thickness is currently not available with satellite systems. This study examined the possibility of obtaining thickness information from passive microwave data. Since microwave radiometric signals from sea-ice strongly reflect physical conditions of a layer near the ice surface, we study how the brightness temperature changes during the early stages of ice growth. We examined the extent to which the relationships of thickness with brightness temperature and with emissivity hold for thin sea-ice, approximately <0.2 -0.3 m in thickness. This was done by taking advantage of near concurrent measurements of sea-ice thickness in the Sea of Okhotsk from a ship and passive microwave radiometry from an aircraft. The results show that the brightness temperature and emissivity increase with thickness in a frequency range of 10-37 GHz for new ice types. The relationship is more pronounced at lower frequencies and at horizontal polarization. We also established an empirical relationship between ice thickness and salinity in the layer near the ice surface from a field experiment, which qualitatively support the idea that changes in the near-surface brine characteristics contribute to the observed dependence of brightness temperature with thickness. Our results suggest that for thin ice, passive microwave radiometric signals contain ice thickness information. Such capability would considerably enhance our ability to assess heat and salinity fluxes from sea ice as well as assess the areal extent of new ice types.

Significant Findings:

One of the critical parameters needed for mass balance and process studies in sea ice covered regions is ice thickness. This study examined the possibility that thickness information can be derived from passive microwave data. We examined the extent to which the relationships of thickness with brightness temperature and with emissivity hold for thin sea-ice (approximately <0.2 -0.3 m), and how those relationships may be related to the time dependent changes in brine content and associated modification of dielectric properties. This was done by taking advantage of near concurrent measurements of sea-ice thickness in the Sea of Okhotsk from a ship and passive microwave radiometry from a NASA P3 aircraft. The results show that the brightness temperature and emissivity increase with thickness in the frequency range of 10-37 GHz but only for new ice types. The relationship is more pronounced at lower frequencies and at horizontal polarization. We also established an empirical relationship between ice thickness and salinity in the layer near the ice surface from a field experiment, which qualitatively support the idea that changes in the near-surface brine characteristics contribute to the observed dependence of brightness temperature with thickness. Our results suggest that for thin ice, passive microwave radiometric signals contain information associated with ice thickness. Such capability would considerably enhance our ability to assess heat and salinity fluxes from sea ice as well as assess the areal extent of new ice types.

Thin Sea-ice Thickness as inferred from Passive Microwave and In Situ Observations

Kazuhiro Naoki[1], Jinro Ukita[1], Fumihiko Nishio[1,2], Masashige Nakayama[3], Josefino C. Comiso[4], and Al Gasiewski[5]

[1] *Graduate School of Science and Technology, Chiba University, Chiba, Japan*

[2] *Center for Environmental Remote Sensing, Chiba University, Chiba, Japan*

[3] *Kushiro Children's Museum, Hokkaido, Japan*

[4] *NASA Goddard Space Flight Center, Maryland, USA*

[5] *NOAA Earth System Research Laboratory, Colorado, USA*

Submitted to JGR-Ocean for the special issue on "Large Scale Characteristics of the Sea Ice Cover from AMSR-E and other Satellites."

Abstract

Since microwave radiometric signals from sea-ice strongly reflect physical conditions of a layer near the ice surface, a relationship of brightness temperature with thickness is possible especially during the early stages of ice growth. Sea ice is most saline during formation stage and as the salinity decreases with time while at the same time the thickness of the sea ice increases, a corresponding change in the dielectric properties and hence the brightness temperature may occur. This study examines the extent to which the relationships of thickness with brightness temperature (and with emissivity) hold for thin sea-ice, approximately <0.2 -0.3 m, using near concurrent measurements of sea-ice thickness in the Sea of Okhotsk from a ship and passive microwave brightness temperature data from an over-flying aircraft. The results show that the brightness temperature and emissivity increase with ice thickness for the frequency range of 10-37 GHz. The relationship is more pronounced at lower frequencies and at the horizontal polarization. We also established an empirical relationship between ice thickness and salinity in the layer near the ice surface from a field experiment, which qualitatively support the idea that changes in the near-surface brine characteristics contribute to the observed thickness-brightness temperature/emissivity relationship. Our results suggest that for thin ice, passive microwave radiometric signals contain, ice thickness information which can be utilized in polar process studies.

1. Introduction

The seasonal sea-ice accounts for about 55% and 80% of the sea-ice covers in the Northern and Southern Hemispheres, respectively [Gloersen et al., 1992; Zwally et al., 2002; Cavalieri et al., 2003]. This implies that globally a significant part of sea-ice undergoes the stage of thin ice formation one point or another within a seasonal cycle. It is estimated that the amount of heat flux through sea-ice of thickness <0.5 m is 1 or 2 orders of magnitude higher than that through thicker ice types [Maykut, 1978]. In this context, it is highly significant that regions with critical climatic importance such as the sub-polar North Atlantic and the Southern Ocean where dense water formation occurs are covered with seasonal sea-ice. Model simulations also indicate that anomalous sea-ice cover and thus heat fluxes could influence large-scale atmospheric circulation [Honda et al., 1999; Alexander et al., 2004]. From these considerations, accurate information on temporal and spatial distributions of thin ice is of significant importance to regional- and basin-scale heat budgets and atmosphere-ocean interaction. Despite the importance of thin ice it is difficult to obtain exact information on its thickness and spatial coverage. It remains a great challenge to derive thickness from satellite remote sensing. For altimeter measurements, necessary conversion from sail height to total thickness makes it difficult to estimates thickness for thin ice [Kwok et al., 2004]. It is also difficult to attain thickness information from passive microwave radiometry since the emission depth is limited within a layer of the top few centimeters, which depends on the wavelength of the radiation.

Notwithstanding, previous work suggest that microwave radiometric signals carry information on

ice thickness for thin ice, which is in this study referred to as ice with a thickness <0.3 m that includes nilas (thickness <0.1 m) and young ice (0.1-0.3 m of thickness) according to the WMO nomenclature [2006]. Troy et al. [1981] report that the emissivity increases from nilas to young and to first-year ice (>0.3 m) (see their Figure 7). Tucker et al. [1991] also present similar results (see their Figure 8), while Eppler et al. [1992] summarize results from various field and laboratory experiments (see their Table 4.1). More recently, algorithms are developed for classification of thin ice, e.g. Cavalieri [1994], and for estimation of thin ice thickness, e.g. Drucker [2003] and Martin et al. [2004, 2005], based on the observation that a polarization ratio and a related brightness temperature ratio between vertical and horizontal polarization depend on thickness. While those studies consistently found the relationship between microwave radiometry and thickness, many of the field observations were not accompanied with exact information on thickness [Grenfell et al. 1992]. Instead observations were often made with respect to sea-ice types. Ambiguities also remain due to a low spatial resolution of space-borne measurements. Many of the previous observations suffer from ambiguities associated with the presence of open water areas and with a mixture of different ice types. What is needed is a focused field experiment on thin sea-ice to measure passive microwave radiometry and thickness concurrently, which provides complementary information to laboratory experiments [e.g. Grenfell and Comiso, 1986].

With this background the purpose of this study is to examine the relationship between the emissivity and thickness with a focus on the effects of changing brine distribution on thin ice. In particular, we examine the following questions: How robust is the relationship between passive microwave signature and thickness as has been reported previously, and how does it stand in other regions, which have not been previously sampled. Is there any relationship between salinity in the layer near the ice surface and thickness in a field condition? If so, how much of the emissivity-thickness relationship is accounted for by emissivity dependence on brine characteristics? In order to address these questions, we analyzed data from concurrent airborne radiometric measurements with a field experiment which include thickness measurements from the ship in the Sea of Okhotsk in February 2003.

2. Experiment description

2.1 Aircraft and ship observations

Since 1995, sea-ice and hydrographical observations have been made in the southernmost region of the Sea of Okhotsk using the icebreaker P/V Soya of the Japan Coast Guard [Ukita et al., 2000]. During the 2003 cruise, from February 6 to 15, continuous survey on sea-ice conditions was conducted from the ship (see Figure 1a for the location of the study area). In addition, passive microwave measurements were made from NASA's P3-B flying over the region on February 7. Figure 1b shows the map of the observed brightness temperatures from the aircraft with ship's track indicated by the black line. As seen in an Aqua/MODIS (Moderate Resolution Imaging Spectroradiometer) image (Figure 1c) taken at 10:45 of the

local time the sky was in clear condition, and the region was covered with sea-ice with ice floes of various sizes (see the details of description on ice conditions in the accompanying paper, Nishio et al. of this issue).

The P3-B flew from the Yokota Air Force Base in Japan and passed over the ship at 11:02 of the local time at the altitude of 6000m. Mounted on the aircraft, the scanning microwave radiometer, Polarimetric Scanning Radiometer (PSR), measured brightness temperatures at the center frequencies of 10.7, 18.7, 21.5, 37.0, and 89.0 GHz and at both horizontal and vertical polarizations [Piepmeier and Gasiewski, 1996]. The size for the field of view was approximately 250 m for 37 GHz, and the scanning swath was approximately 20 km. Prior to analysis, the PSR data were preprocessed and resampled to make gridded data with the resolution of 150 m. Figure 2 presents time series of the brightness temperatures at 18.7 and 37 GHz for both horizontal and vertical polarizations, which were constructed from the gridded data along ship's track using navigational information.

At the ship, meteorological variables including wind direction and speed, air temperature, and humidity were recorded. Most importantly, sea-ice conditions were continuously recorded using a video camera system, which consists of three cameras and a recorder (see Toyota et al. [1999] for the description of the system). Two cameras mounted at the bow and on the mast look into the forward direction, which provide visual information on sea-ice conditions. In particular they inform us with the extent of homogeneity in sea-ice conditions around the ship. The downward looking camera mounted at the side of the ship recorded images of the broken sea-ice, from which sea-ice thickness was estimated. Figure 3 presents thus obtained sea-ice thickness distribution on February 7 (the day of the concurrent measurements).

2.2 Site selection

Thickness measurements from the ship were made throughout the day, while PSR measurements were made at around 11:02 in the local time. This means that if ice motion is substantial simple correspondence between PSR pixels and ship's track based on their positions (e.g. latitude and longitude information) would not guarantee matching between the ship and aircraft measurements. In order to avoid sampling errors associated with potential mismatch, we employed the following procedure. First, candidates for study sites were selected by visual inspection of the recorded video scene as well as a pair of MODIS and PSR images. In particular, we chose sites that meet the following criteria: (1) Sea-ice concentration is nearly 100%; (2) The ice condition including thickness is close to constant; (3) The above two conditions are satisfied over the distance of at least about 300 m along the track's direction and within the view from the ship. Second, we co-located those potential sites in the visible MODIS image (e.g. Figure 1b). This step was made possible by calm weather conditions. The potential sites were easily identified in the MODIS image based on ship's navigational data. In fact, the average wind speed during the observation period was approximately 1.5 m/s. This translates to ice motion of 160 m per hour, assuming 3 percent as

the ratio of ice to wind speeds. Since at this wind speed the nonlinear behavior of the steady-state momentum balance would give a smaller fraction this estimate is taken as a basis for maximum search distance in identifying targeted sites in the MODIS image (Figure 1c). The third step was to co-locate those sites found in the MODIS image in the PSR brightness temperature image (e.g. Figure 1b) by a means of a visual inspection. This step was also made possible due to a rather short interval between the times of the MODIS and PSR observations, e.g. 17 minutes. The fourth step was to chose PSR grids for brightness temperature measurements based on the information gained through the above steps.

By following the above steps, we were able to measure thickness and brightness temperature from the same floe or a general area with highly homogeneous ice conditions. Our analysis indicates that this procedure, though not perfect, provides us with reasonably accurate matching between the locations of the PSR measurements and thickness measurements from the ship. In fact, based on a four-way comparison between ship's video and navigational data, MODIS and PSR images, we confirmed that there was no substantial ice motion for Sites B and C. These sites represent the smallest in study area (short segments in ship's track) and were observed 3 and 4 hours prior to the time of the PSR observation. Hence, the procedure appears to be reasonably valid.

It turns out that 6 study sites are chosen. The mean sea-ice thickness ranges from <0.05 m to about 0.3 m (Figure 1b and 1c indicate their locations in the brightness temperature map and the MODIS image, respectively). The mean ice thickness at Site B to F is 0.068 m, 0.111 m, 0.185 m, 0.272 m, 0.322cm, respectively (Table 1 gives the summary statistics). The thickness at Site A could not be determined from the video analysis, because it is only capable of estimating thickness >0.05 m. However, from the recorded video image it is confirmed that sea-ice was present at Site A. Thus the nominal thickness of 0.025 m is given for Site A. The sample size for thickness measurements varies from 12 to 99 depending on sites.

3. Results

3.1 Thickness versus brightness temperature

Figure 4 plot the mean brightness temperatures measured at the aircraft against the mean sea-ice thickness measured for the six study sites for five frequencies 10.7, 18.7, 21.5, 37.0, and 89.0 GHz and for horizontal and vertical polarizations. A number of features are noted. (1) At all frequency except at 89 GHz, the brightness temperature increases with ice thickness for a thickness range up to 0.272 m. (2) At 89 GHz, the brightness temperature peaks at <0.2 m and decreases for the thickness >0.2 m. (3) The brightness temperature is lower for the horizontal polarization, and the difference between horizontal and vertical polarizations becomes smaller with increasing thickness (depolarization). (4) Except at 89 GHz, the brightness temperature is lower for lower frequency bands. (5) The positive relationship between the ice thickness and the brightness temperature is more pronounced with a steeper slope for the horizontal polarization and at lower frequencies (e.g. 10.7 GHz).

3.2 Thickness versus emissivity

To account for the dependence of the brightness temperature on physical temperature of an emitting medium, it is desirable to discuss microwave signatures in terms of emissivity. To illustrate, Figure 5a and 5b (horizontal and vertical polarizations) plot emissivity against thickness for 6 sites and for 18.7 and 37 GHz. The plotted values are the brightness temperatures of Figure 4 divided by the physical temperature of 266.15 Kelvin (-7°C), which is the in-situ ice surface temperature at the time of the PSR overpass. A number of features are noted in Figure 5a and 5b: (1) The emissivity increases with ice thickness within the thin category; (2) Given an ice type and thickness, the emissivity is higher for the vertical polarization; (3) The variation in emissivity due to different polarizations diminishes with increasing thickness; and (4) The variation in emissivity due to different polarizations is larger than that due to different frequencies.

There are uncertainties in the above estimates associated with the variations in ice thickness and brightness temperatures as seen in Table 1. Nevertheless, the thickness variation within each site is small enough such that there is no overlap between horizontal error bars among different sites/thickness except for the thickest point (Site F). The variation in the brightness temperature is also small. In converting from the brightness temperature to the emissivity, the values of the brightness temperatures are divided by the physical temperature. Ideally, the correct temperature to use is one that represents physical temperature of the emitting layer. This means that the temperature gradient within the ice column needs to be taken into account. In the absence of such information, we made a sensitivity analysis using the temperature rage of -7°C to -1.8°C. As it turned out the maximum difference in emissivity when using -1.8°C instead of 7°C is about 0.02. Based on the above analysis, the sum of the values associated the variations in brightness temperatures within sites and 0.02 due to the temperature variation in the ice column are used for the size of the error bars.

In placing the above results in the context of the previous results, Figure 5c and 5d plot values of emissivity, which are compiled from other studies (the sources are found in the works of Troy et al. [1981], Tucker et al.[1991], and Eppler et al. [1992]). Many of those results are with respect to ice types such as nilas, new and young ice without thickness information. When exact thickness is not available, the representative (mean) thickness of each ice type is used. For example, 0.05 m and 0.2 m represent the thickness of nilas (< 0.1m) and young ice (0.1-0.3 m), respectively. Comparison of Figure 5a with 5c and Figure 5b with 5d shows a high degree of consistency, and common features are clearly identified. The most obvious feature to note is that the emissivity increases with ice thickness within the thin-end, which is more pronounced for the horizontal polarization and for a lower frequency, e.g. at 18.7 GHz. There are however some differences. For example, for the horizontal polarization our values are higher than the compiled for a thickness <0.1 m.

4. Brine hypothesis

4.1 Salinity-thickness relation

For thin sea-ice evidence emerge that passive microwave radiometric signals contain, though not direct, information on ice thickness. The brightness temperature increases with thickness when ice is approximately thinner than 0.2 m. This relationship has been observed consistently over different geographical locations including the central Arctic, the Bering Sea, the Greenland Sea, and the Sea of Okhotsk. This wide appearance is taken as an indication that causes for the relationship are fundamental to underlying sea-ice physics. Different factors such as influences from snow, roughness, brine and temperature may contribute to this behavior in sea-ice radiometry. However, given the consistency of the behavior despite a range of different physical environments encountered in different regions, it may be argued that snow and temperature alone would not account for the observed relationship. This is because the amount of snow and temperature are highly variable in time and space due to different weather and climatic conditions. Our analysis also suggests that the uncertainty in estimating emissivity associated with the vertical temperature variation is small. It is unlikely that the low emissivity of the ocean beneath sea-ice would account for the relationship either, because the thickness range for which the emissivity-thickness relation is observed exceeds the penetration depth. Having ruled out snow, temperature and the oceanic influences, we hypothesize that changes in brine with time and/or with thickness in freezing condition would be a main factor for the relationship (see the discussions in Troy et al. [1981], Tucker et al. [1991] and Epper et al. [1992]).

A physical basis for this brine hypothesis is observed dependence of salinity on ice thickness. It has been known that there is a tendency that near-surface salinity decreases with the total thickness as a result of brine drainage [Cox and Weeks, 1974; Ukita et al., 2000]. In general, salinity near the ice surface tends to decrease in growing conditions and with time. We then explore the idea that the observed thickness-brightness temperature relationship would reflect changes in dielectric properties associated with changes in brine characteristics. Ideally, testing this idea requires gaining information on brine in the layer close to the surface concurrently with microwave radiometric and thickness measurements.

As a step towards testing this idea, we extended a field program in which we made in-situ measurements of salinity of the near-surface layer and ice thickness at Lake Saroma [see Figure 7 of Nakamura et al., 2006]. The lake is located adjacent to the Sea of Okhotsk (Figure 1a), thus essentially sharing the same meteorological conditions. In addition Lake Saroma is connected to the Sea of Okhotsk with channels, which allows us to conduct in situ measurements. In Figure 6 the bulk salinity of the top 5cm near the ice surface (when snow is present it is removed before taking an ice sample) is plotted against thickness. There appears a negative relationship between thickness and bulk salinity.

In order to approximate functional dependence of near-surface salinity on thickness, least square regression is applied with two models. One is a linear model, which gives an estimated relationship as

$$S=18.55+0.3678h \quad (1a)$$

where S and h denote bulk salinity of the top 0.05 m of the ice column and thickness in centimeter. The other is an exponential model resulting in

$$S=21.404e^{-0.0355h} \quad (1b)$$

The above regression models explain 67% and 56% of the variance, respectively.

4.2 Modeling temperature and brine effects

In an attempt to quantify the extent to which the change in brine gives rise to change in emissivity via modification of dielectric properties, we examine the way in which a change in brine modulates emissivity using the formula by Hoekstra and Cappillino [1971]. Let e denotes the emissivity of sea-ice, Γ the Fresnel refection coefficient, θ the incidence angle from the nadir, and ε the dielectric constant.

$$e(\theta)=1-\left|\Gamma(\theta)\right|^2 \quad (2)$$

The Fresnel refection coefficient is expressed as

$$\Gamma(\theta)=\frac{\cos\theta-\sqrt{\varepsilon-\sin^2\theta}}{\cos\theta+\sqrt{\varepsilon-\sin^2\theta}} \quad (3a)$$

for the horizontal polarization and

$$\Gamma(\theta)=\frac{\varepsilon\cos\theta-\sqrt{\varepsilon-\sin^2\theta}}{\varepsilon\cos\theta+\sqrt{\varepsilon-\sin^2\theta}} \quad (3b)$$

for the vertical polarization. The dielectric constant for sea-ice, ε_{si} takes a form

$$\varepsilon_{si}=\varepsilon'_{si}+\varepsilon''_{si} \quad (4)$$

where the first and second terms are real and imaginary parts of the dielectric constant. They can be modeled [Hoekstra and Cappillino, 1971] as

$$\varepsilon'_{si}=\frac{\varepsilon'_i}{1-3V_b} \text{ and} \quad (5a)$$

$$\varepsilon''_{si}=V_b\varepsilon''_b \quad (5b)$$

where ε'_i (here assumed to take 3.15 as its value) is the real part of the dielectric constant for pure ice, ε''_b is the imaginary part of the dielectric constant for brine, and V_b is the brine volume. They are functions of frequency and temperature (see Strogyn [1971] for discussions on ε''_b and Ulaby [1986] for more general discussions). The brine volume can be related to salinity and temperature as

$$V_b = 10^{-3} S\left(\frac{-49.185}{T} + 0.532\right) \qquad (6)$$

where S and T and bulk salinity and temperature with S in ppt, T in the range of -0.5 to -22.9°C, and V_b is brine volume in ppt [Frankenstein and Garner, 1967]. Using (2) to (6) and the incidence angle of 55 degrees, the emissivity of sea ice can be modeled as a function of temperature and salinity. Now using the surface temperature of -7°C and estimated linear and exponential thickness-salinity relationships (Equation 1a and 1b), a thickness-emissivity relationship is modeled and compared with observed values (see Figure 7). The model results are qualitatively in agreement with the observations. In particular, both linear and exponential models explain a positive relationship between the brightness temperature and thickness. It is also confirmed that the models could explain observed dependence on polarization and frequencies (e.g. Figure 4 and 5). It is however noted that nonlinear behavior in PSR and other measurements especially towards the thin-end is only seen with an exponential model (1b). The above results suggest that the observed dependence of the brightness temperature and emissivity on thickness for thin ice is partly explained by changes in brine distribution with age and thickness of ice, although other factors such as snow and roughness may contribute.

5 Discussions

The above results support the notion that for thin ice, the brightness temperature and emissivity of seasonal sea ice increase with ice thickness. Furthermore, the results from both field and modeling studies suggest that a plausible explanation for this relationship lies in changing brine distribution near the surface, which results in the modification of dielectric properties and thereby leading to dependence of microwave radiometry on ice thickness.

What it follows we discuss the present results in conjunction with previous studies on a combined problem of classification of thin ice and estimation of its thickness. At present there are two main approaches to the problem. One approach is based on thermal infrared data, in which ice thickness is estimated using the condition that the heat flux through the ice column equals to the atmospheric flux [e.g. Yu and Rothrock, 1996; Drucker et al. 2003]. The second approach is based on passive microwave radiometry, in which microwave polarization information is utilized for classification of thin ice [Cavalieri, 1994] and for thickness estimation [e.g. Drucker et al., 2003; Martin et al., 2004, 2005]. To describe the second approach, let us define a polarization (PR) ratio and a spectral 339 gradient (GR) ratio as

$$PR = [T_b(19V) - T_b(19H)]/[T_b(19V) + T_b(19H)] \qquad (7a)$$

$$GR = [T_b(37\,V) - T_b(19V)]/[T_b(37\,V) + T_b(19V)] \qquad (7b)$$

where T_b denotes the brightness temperature, and frequency and polarization are indicated inside 346 the parentheses.

Based on a series of tank and field experiments Wensnahan et al. [1993] find that PR changes its value as ice grows. In particular they report a reversed sequence in PR values, i.e. an initial decrease followed by an increase in PR when ice grows to a thickness of about 0.06 m. Besides this, they find that the value of PR tends to be around 0.1 by the time ice grows to about 0.05 m. It is significant that this value is between the PR values of the open water and the first-year ice, which essentially serves as a basis for the Cavalieri's thin ice algorithm [Cavalieri, 1994]. As he states the question of this depolarization (decreasing PR towards the unity) with ice thickness is not yet resolved. A particular difficulty arises from the fact that combined information of radiometry and thickness in the seasonal sea ice zone is scarce. And even if available, ambiguities remain as to possible biases from a mixture of different ice types and the open water.

Keeping this background in mind, Figure 8 shows the values of PR and GR calculated based on PSR measurements along with the thickness information. It is noted that PR values decrease with thickness except for the thickest case (0.32 m at Site F). In comparison, GR values are relatively unchanged and close to be zero. These results are highly consistent with the previous observations compiled in Table 1 of Cavalieri [1994]. More importantly, our results are from the observations with a less amount of ambiguities in terms of the mixing question.

More recently, Martin et al. [2004] introduce an index called the Special Sensor Microwave/Imager (SSM/I) 37V/H ratio R_{37} defined as

$$R_{37} = [T_b(37\ H)]/[T_b(37\ H)] \qquad (8)$$

They derived an empirical relationship of this ratio with ice thickness estimated from Advanced Very High Resolution Radiometer (AVHRR) data using the method described in Drucker et al. [2003]. The values of R_{37} calculated from our PSR measurements range between 1.03 (Site D and E) to 1.31 (Site A). Qualitatively this range and its dependence on thickness (a negative relationship between thickness and R_{37}) are in agreement with those found in Martin et al. [2004]. It is also noted that R_{19}, which is the 19 GHz counterpart to R_{37}, has a wider range (1.05-1.54).

To further compare our results with others, we map PR for 18 GHz and R_{18} using AMSR-E (The Advanced Microwave Scanning Radiometer - Earth Observing System) data for the entire Sea of Okhotsk on February 7, 2003 (Figure 9). Here in order to minimize influences from the open water the only grids, for which ice concentration are >80%, are considered [e.g. Comiso et al., 2003]. Regions with high values, which are indicative of thin ice, are noted in both maps. One such an area is located along the northern coast, which is known to develop coastal polynyas [Martin et al., 1998; Shcherbina et al., 2004]. Other

areas include two south-faced bays along the eastern coast of the Sakhalin Island, which are also known to be polynyas due to prevailing northerly winds and local topography. In all, those features are what we expect for a spatial pattern of the thin ice distribution for this region.

Now focusing on our study region defined by the PSR swath (Figure 1), Table 2 presents statistics on PR and *R* values calculated from PSR measurements and geographically matching AMSR-E data. The minimum values of PR and *R* are similar between AMSR-E and PSR data (here the sample sizes are so different that standard statistical tests are not applied). The mean values are also close between the distributions derived from the two data sets. The maximum of PR values from PSR is notably larger (0.228) than that from AMSR-E. It is highly consistent with the value (0.275) found for the open water in Cavalieri [1994]. Similarly, the maximum of *R* values for PSR (1.593) is larger than that for AMSR-E. On the basis of the above comparisons, it appears that the present PSR measurements provide the same radiometric information on thin ice thickness as the AMSR-data. Given in situ thickness information and high spatial resolution, our data serve for the purpose of validation and cross-referencing among different indices developed for classification of thin ice and estimation of its thickness.

6. Conclusions

The present results provide much needed ground-truth for the investigation of the relationship between passive microwave radiometry and ice thickness. In particular, they show the presence of the brightness temperature-thickness relationship for thin ice with reasonably accurate information on thickness and without ambiguities that might otherwise arise from a mixture of different ice types. Hence, they provide a physical basis for the algorithms of thin ice classification and estimation of thin ice thickness [Cavalieri, 1994; Drucker et al., 2003; Martin et al., 2004, 2005].

Our results also point out the importance of near-surface brine distribution as a key factor for the dependence of microwave radiometry on thin ice thickness, which places a strong need for future in-site and concurrent measurements on radiometry, thickness, and brine characteristics. One way to extend our results is to consider the seasonal sea-ice cover in the Southern Ocean, for which efforts should be directed towards obtaining knowledge on brine distribution of sea ice under flooding conditions. Lastly but not least importantly, it is needed to gain more knowledge on dielectric properties of sea ice in field conditions.

Acknowledgments: We are grateful to the Japanese Coast Guard, and the crews of the Soya for their assistance during the cruise. We also thank J. Inoue, K.Tateyama, T. Toyota, and S. Watanabe for their assistance during the cruise and K. Nakamura and H. Wakabayashi for helpful discussions. The research was funded in part by NASA's Cryospheric Sciences Program. Corresponding author: Dr. Jinro Ukita, Chiba University, jukita@faculty.chiba-u.jp.

References

Alexander, M. A., U. S. Bhatt, J. E. Walsh, M. S. Timlin, J. S. Miller, and J. D. Scott, The atmospheric response to realistic Arctic sea ice anomalies in an AGCM during winter, *J. Clim.*, **17**, 890-905, 2004.

Cavalieri, D. J., Microwave technique for mapping thin sea ice, *J. Geophys. Res.*, **99**, 12,561-12,572, 1994.

Cavalieri, D. J., C. L. Parkinson, and K. Y. Vinnikov, 30-Year satellite record reveals contrasting Arctic and Antarctic decadal sea ice variability, *Geophys. Res. Lett.*, **30**, 1029/2003GL018031, 2003.

Comiso, J., D. Cavalieri, and T. Markus, Sea ice concentration, ice temperature, and snow depth using AMSR-E data, *IEEE Transactions on Geoscience and Remote Sensing* 41(2): 243-252, 2003.

Cox, G.F.N. and W.F. Weeks, Salinity variations in sea ice, *J. Glaciol.*, **13**, 109–120, 1974.

Drucker, R., S. Martin, and R. Moritz, Observation of ice thickness and frazil ice in the St. Lawrence Island polynya from satellite imagery, upward looking sonar, and salinity/temperature moorings, *J. Geophys. Res.*, **108**, 3149, doe:10.1029/2001JC001213, 2003.

Eppler, D. and 14 other co-authors, Passive microwave signature of sea ice, Chap 4 in *Microwave Remote Sensing of Sea Ice*, Geophys. Monogr. 68, pp. 47-71, AGU, Washington D. C., 1992.

Frankenstein, G. and R. Garner, Equations for determining the brine volume of sea ice from –0.5°C 502 to –22.9°C, *J. Glaciol.*, **6**, 943–944, 1967.

Gloersen, P., W. J. Campbell, D. J. Cavalieri, J. C. Comiso, C. L. Parkinson, and H. J. Zwally, Arctic and Antarctic sea ice, 1978-1987: Satellite passive-microwave observations and analysis, *NASA, SP-511*, pp. 290, 1992.

Grenfell, T. C., and J. C. Comiso, Multifrequency passive microwave observations of first-year sea ice grown in a tank, *IEEE Trans. Geosci. Remote Sens.*, GE-24, 826-831, 1986.

Grenfell, T. C., D. J. Cavalieri, J. C. Comiso, M. R. Drinkwater, R. G. Onstott, I. Rubinstein, K. Steffen, D. P. Winebrenner, Considerations for microwave remote sensing of tin sea ice, in *Microwave Remote Sensing of Sea ice*, Geophys. Monogr. Ser., vol 68, F. Carsey, ed., pp.291-301, AGU, Washington D. C., 1992.

Hoekstra, P. and P. Cappillino, . Dielectric properties of sea and sodium chloride ice at UHF and microwave frequencies, *J. Geophys. Res.*, **76**, 4922-4931, 1971.

Honda, M., K. Yamazaki, H, Nakamura, and K. Takeuchi, Dynamic and thermodynamic 520 characteristics of atmospheric response to anomalous sea-ice extent in the Sea of Okhotsk, *J.* 521 *Clim.*, **13**, 617-633, 1999.

Kwok, R., H. J. Zwally, and D. Yi, ICESat observations of Arctic sea ice: A first look, *Geophys. Res. Lett.*, **31**, L16401, doi:10.1029/2004GL020309, 2004.

Martin, S., R. Drucker, and K. Yamashita, The production of ice and dense shelf water in the Okhotsk Sea polynyas, *J. Geophys. Res.*, **103**, 27,771– 27,782, 1998.

Martin, S., R. Drucker, R. Kwok, and B. Holt, Estimation of the thin ice thickness and heat flux for the Chukchi Sea Alaskan coast polynya from Special Sensor Microwave/Imager data, 1990-2001, *J. Geophys. Res.*, **109**, doi:10.1029/2004JC002428, 2004.

Martin, S., R. Drucker, R. Kwok, and B. Holt, Improvements in the estimates of ice thickness and production in the Chukchi Sea polynyas derived from AMSR-E, *Geophys. Res. Lett.*, **32**, L05505, doi:10.1029/2004GL022013, 2005.

Maykut, G., Energy exchange over young sea ice in the central Arctic, *J. Geophys. Res.*, **83**, 3646-3658, 1978.

Nakamura, K., H. Wakabayashi, S. Uto, K. Naoki, F. Nishio, and S. Uratsuka, Sea-ice thickness retrieval in the Sea of Okhotsk using dual-polarization SAR data, *Ann. Glaciol.*, **44**, 261-268, 2006.

Piepmeier, J.R., and Gasiewski, A.J., Polarimetric Scanning Radiometer for airborne microwave imaging studies, *Proceedings of the 1996 International Geoscience and Remote Sensing Symposium*, 1688-1691, 1996.

Shcherbina, A. Y., L. D. Talley, and D. L. Rudnick, Dense water formation on the northwestern shelf of the Okhotsk Sea: 1. Direct observations of brine rejection, *J. Geophys. Res.*, **109**, C09S08, doi:10.1029/ 2003JC002196, 2004.

Stogryn, A., Equations for calculating the dielectric constant of saline water (Correspondence), *IEEE Trans. Microwave Theory Tech.*, **19**, 733–736, 1971.

Toyota, T., J. Ukita, K. I. Ohshima, M. Wakatsuchi and K. Muramoto, A measurement of sea ice albedo over the southwestern Okhotsk Sea, *J. Meteor. Soc. Japan,* **77**, 117-133, 1999.

Troy, B. E., J. P. Hollinger, R. M. Lerner, and M. M. Wisler, Measurement of the microwave properties of sea ice at 90GHz and lower frequencies, *J. Geophys. Res.*, **86**, 4283-4289, 1981.

Tucker III, W. B., T. C. Grenfell, R. G. Onstott, D. K. Perovich, A. J. Gow, R. A. Shuchman, and L. Sutherland, Sea ice properties in the winter marginal ice zone, *J. Geophys. Res.*, **96**, 4573-4587, 1991.

Ukita, J., T. Kawamura, N. Tanaka, T. Toyota, and M. Wakatsuchi, Physical and stable isotopic properties and growth processes of sea ice collected in the southern Sea of Okhotsk, *J. Geophys. Res.*, **105**, 22083-22093, 2000.

Ulaby, F. T., R. K. Moore, and A. K. Fung, *Microwave Remote Sensing: Active and Passive*, vol III, *From Theory to Applications*, Artech House, Norwood, MA, pp. 1065-2137, 1986.

Yu, Y., and D. A. Rothrock, Thin ice thickness from satellite thermal imagery, *J. Geophys. Res.*, **101**, 25753-25766, 1996.

Wensnahan, M., G. A. Maykut, T. C. Grenfell, and D. P. Winebrenner, Passive microwave remote sensing of thin sea ice using principal component analysis, *J. Geophys. Res.*, **98**, 12,453-12,468, 1993.

WMO Sea Ice Nomenclature, WMO-No.259, WMO, Geneva, 2006.

Zwally, H. J., J. C. Comiso, C. L. Parkinson, D. J. Cavalieri, and P. Gloersen, Variability of the Antarctic sea ice cover, *J. Geophys. Res.*, **107**, 1029-1047, 2002.

Table 1. Summary of thickness and brightness temperature measurements. All values are averages for study sites, A to F. The mean thickness for Site A was denoted as 2.5 cm which was the half the measurement limit of 5 cm. The values inside the parentheses indicate corresponding standard deviations (1σ).

		Site A	Site B	Site C	Site D	Site E	Site F
Mean thickness (cm)		2.5	6.8(±1.1)	11.1(±2.3)	18.5(±3.8)	27.2(±13.7)	32.2(±7.4)
H-pol (K)	10.7GHz	119.1(±1.5)	174.5(±1.3)	190.3(±0.2)	223.7(±1.7)	231.7(±3.6)	217.1(±9.3)
	18.7GHz	137.7(±1.9)	189.7(±0.9)	211.1(±0.1)	231.6(±1.8)	240.4(±3.3)	226.2(±7.0)
	21.5GHz	154.0(±1.5)	197.5(±1.3)	222.5(±0.0)	236.4(±1.5)	244.3(±2.6)	233.7(±6.7)
	37.0GHz	175.1(±3.0)	207.3(±0.3)	235.2(±0.5)	243.2(±1.7)	246.3(±3.0)	244.4(±7.6)
	89.0GHz	196.2(±1.9)	230.3(±0.3)	233.7(±0.3)	237.9(±1.3)	227.6(±1.3)	225.9(±2.8)
V-pol (K)	10.7GHz	196.1(±1.6)	229.3(±0.7)	236.2(±0.2)	249.8(±3.2)	249.5(±0.7)	243.8(±5.1)
	18.7GHz	212.6(±1.4)	239.3(±0.9)	242.0(±0.0)	249.6(±1.3)	253.6(±0.6)	249.7(±1.5)
	21.5GHz	217.6(±1.4)	240.3(±0.5)	244.2(±0.1)	249.4(±1.1)	253.5(±0.6)	250.8(±1.4)
	37.0GHz	230.2(±2.1)	246.3(±0.5)	248.9(±0.5)	252.2(±0.6)	254.9(±0.6)	255.2(±1.1)
	89.0GHz	243.5(±1.5)	247.7(±1.0)	246.9(±0.4)	248.1(±1.5)	238.3(±1.2)	233.6(±3.6)
Number of samples (thickness)		N/A	12	13	99	77	25
Number of samples (PSR grids)		7	3	3	25	23	7

Table 2. Comparison of PR18 and R_{18} values between AMSR-E and PSR data 590 591

	AMSR-E (n = 24)		**PSR** (n = 41777)	
PR18	Range	0.029 - 0.103	Range	0.017 - 0.228
	Mean	0.071	Mean	0.079
R18	Range	1.060 - 1.230	Range	1.034 - 1.593
	Mean	1.154	Mean	1.177

Figure captions

Figure 1. (a) Geographic location of the southern Sea of Okhotsk. The rectangular area indicates the PSR swath. (b) 37 GHz H-polarization image from PSR in gray scale. The black line indicates ship's track. The locations of 6 sites are denoted as A to F. (c) Aqua / MODIS Channel 2 (841-876 nm) image. The locations of the study sites are denoted as in (b).

Figure 2. Time series of brightness temperatures along the flight path, (a) for the horizontal and (b) for vertical polarizations. The heavy lines indicate the times series of 18.7 GHz, and the thin lines for 37.0 GHz. The values on the horizontal axes are approximate distances from the coast of Hokkaido.

Figure 3. Sea ice thickness distribution from the ship's measurements on Feb. 7, 2003. The mean thickness was 0.192 m from 1667 measurements.

Figure 4. Thickness versus brightness temperatures for different frequencies and both horizontal and vertical polarizations. Horizontal and vertical bars indicate one standard deviations of ice thickness and brightness temperatures at each site.

Figure 5. Comparison of thickness-emissivity relationships. (a) and (b) are from our observations, and (c) and (d) are from previous studies. For (c) and (d), mean values are used for different sea-ice types according to the WMO nomenclature. See the text for the discussion on the error bars.

Figure 6. Relationship between sea-ice thickness and surface (top 5 cm) salinity. All data were taken from Lake Saroma over the period from 1996 to 1998 and 2003, 2004 at various locations. The data for a thickness <0.1 m were taken from a pool experiment in Lake Saroma in 2006. Two lines indicate regression lines according to linear and exponential forms.

Figure 7. Comparison of thickness-emissivity relationships between our observations and model results. Diamond and plus symbols indicate the values based on the linear and exponential regression lines in Figure 6.

Figure 8. PR versus GR calculated from PSR measurements for 6 sites. The numerical values in the figure show the mean thickness at each site (e.g. Table 1).

Figure 9. (a) The map of PR values based on AMSR-E observations on February 7, 2003 over the Sea of Okhotsk. (b) The same as (a) but for the vertical to horizontal polarization ratio of brightness temperatures at 18 GHz (r_{18}). The areas with ice concentration <80% are masked out. The color scales indicate corresponding values.

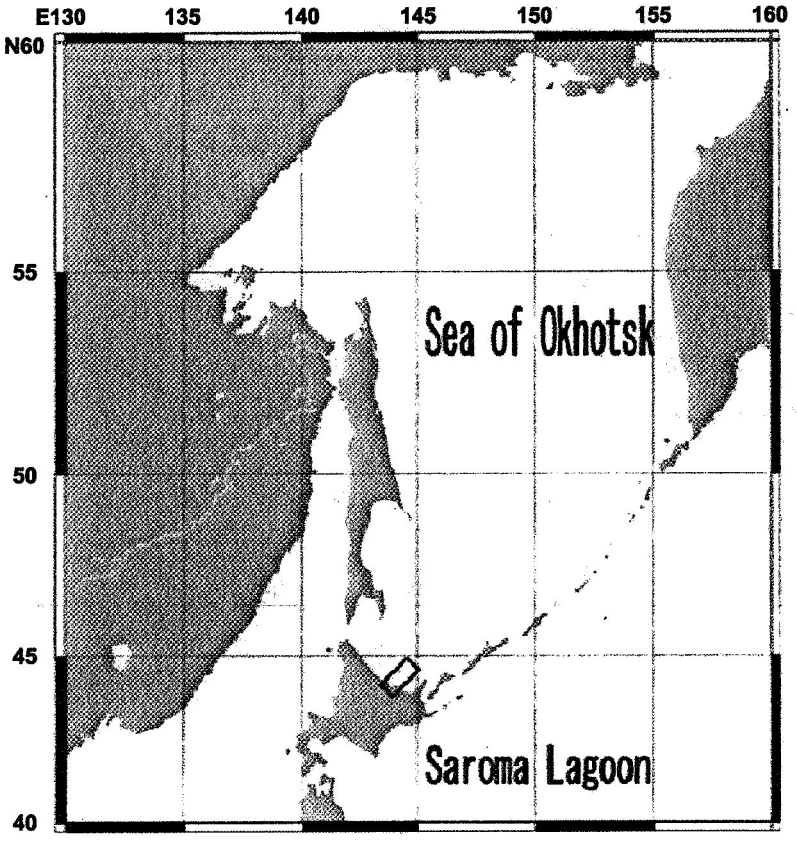
E130
135
140
145
150
155
160
N60
55
50
45
40
Sea of Okhotsk
Saroma Lagoon

Figure 1(a)

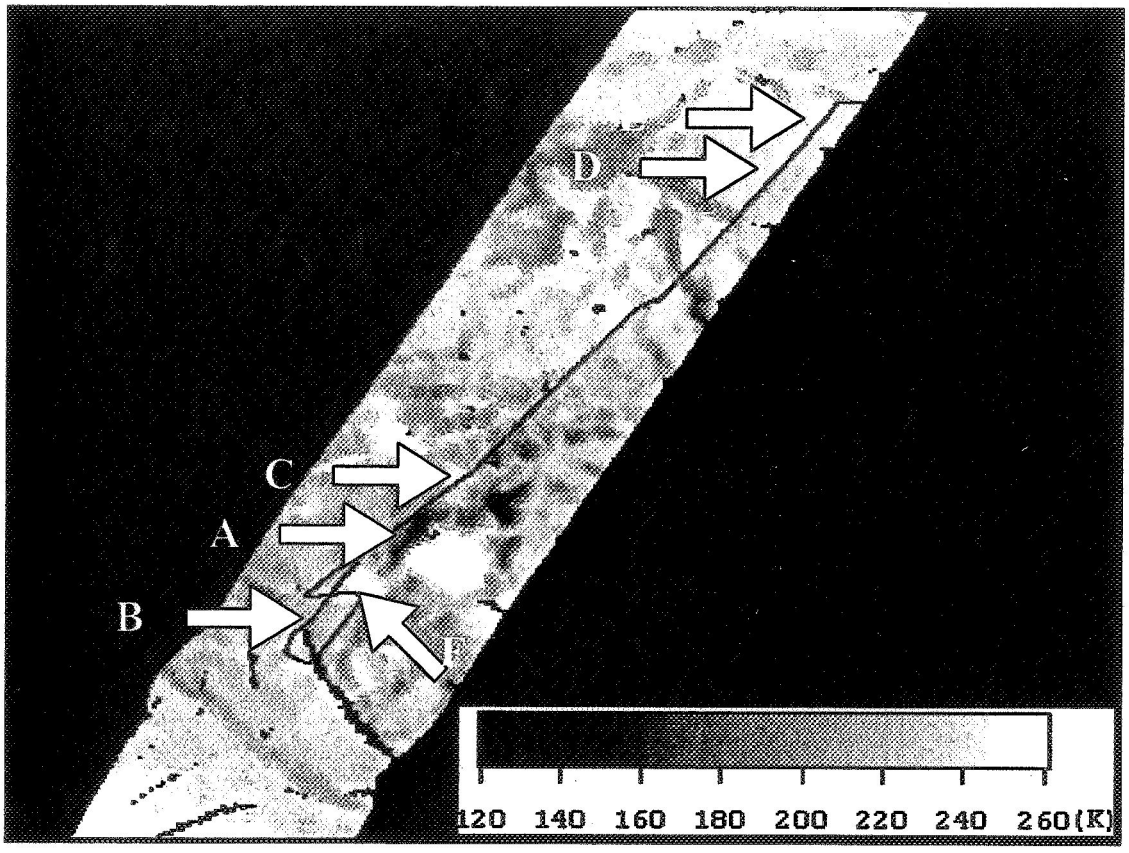

Figure 1(b)

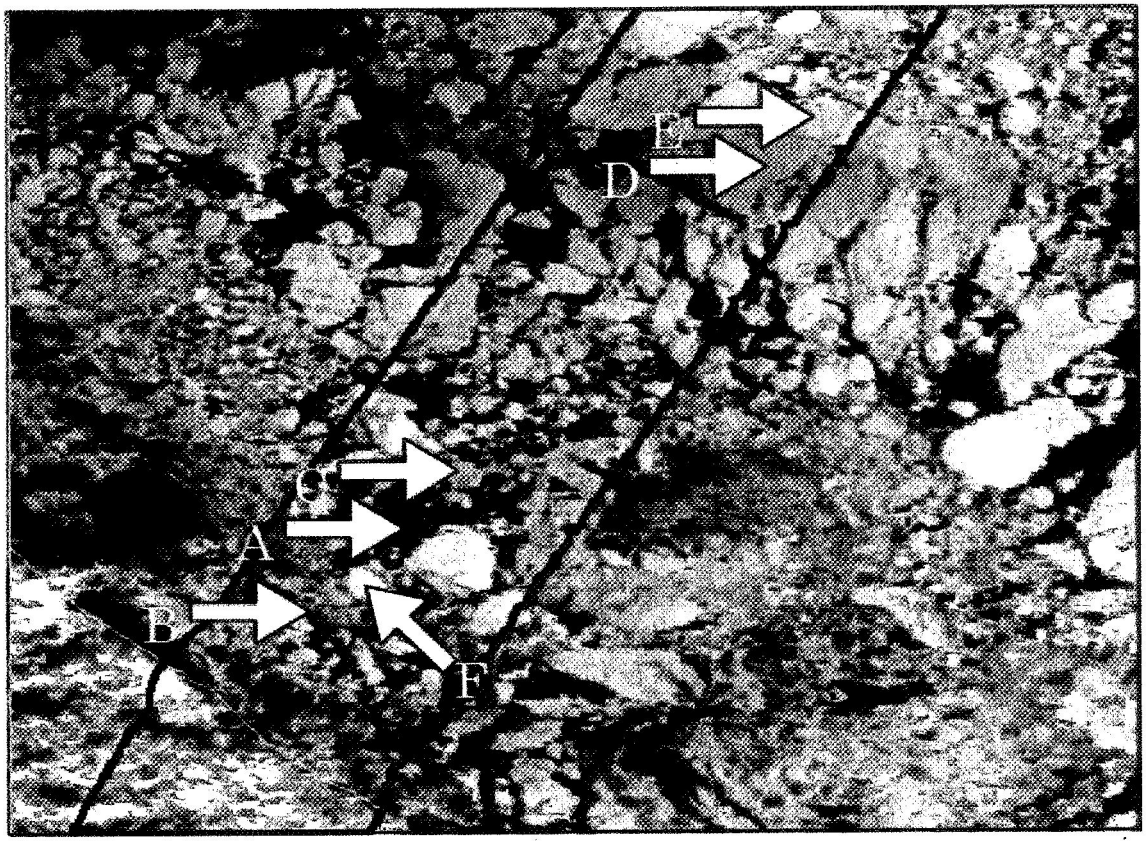

Figure 1(c)

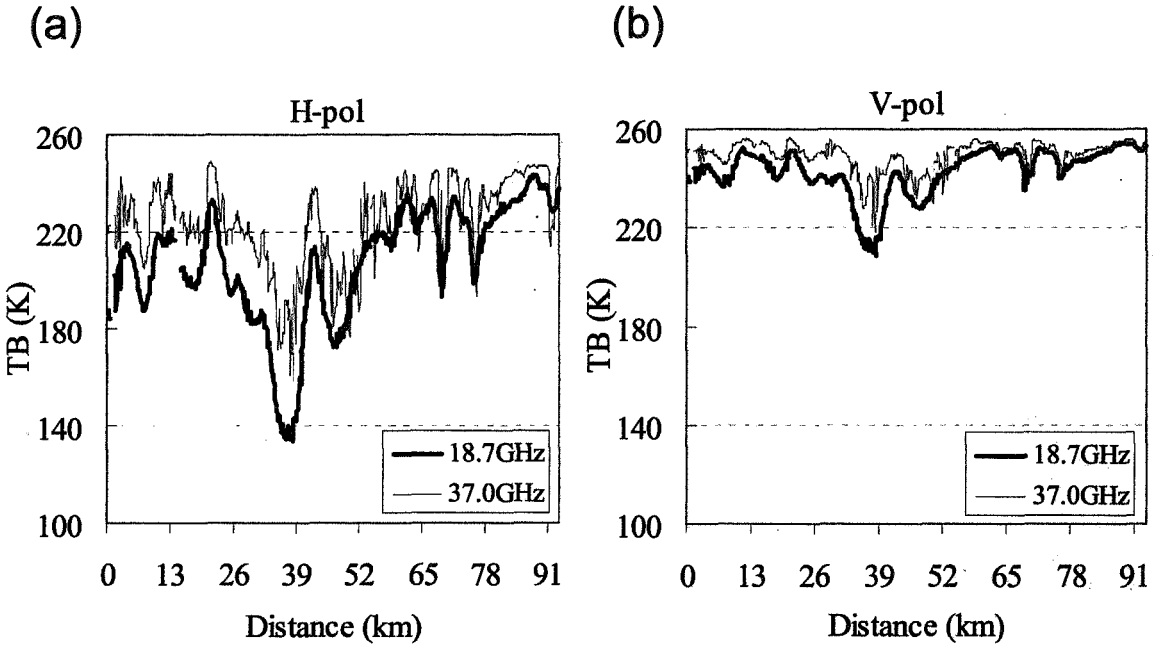
(a)
H-pol
260
220
180
140
100
TB (K)
18.7GHz
37.0GHz
0
13
26
39
52
65
78
91
Distance (km)
(b)
V-pol
260
220
180
140
100
TB (K)
18.7GHz
37.0GHz
0
13
26
39
52
65
78
91
Distance (km)

Figure 2

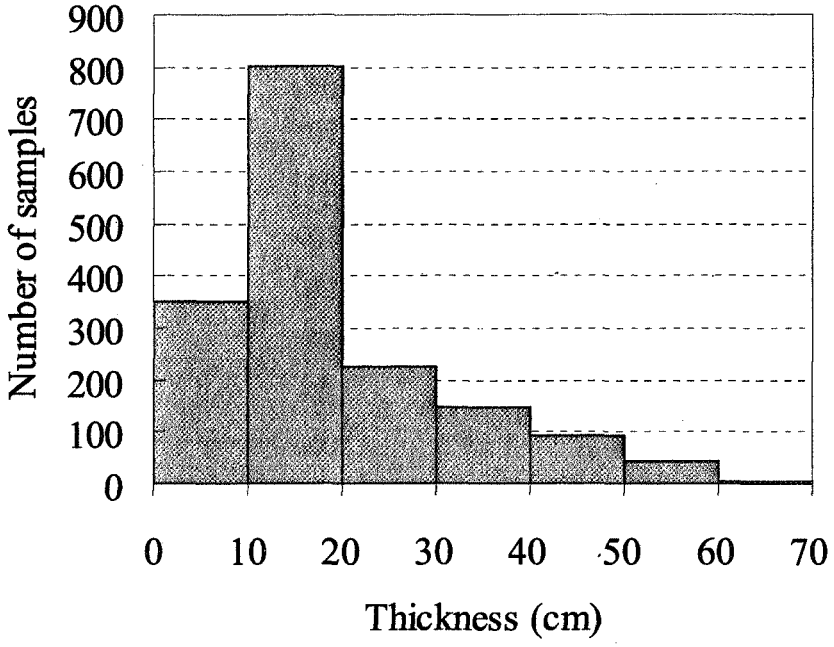
900
800
700
600
500
400
300
200
100
0
Number of samples
0
10
20
30
40
50
60
70
Thickness (cm)

Figure 3

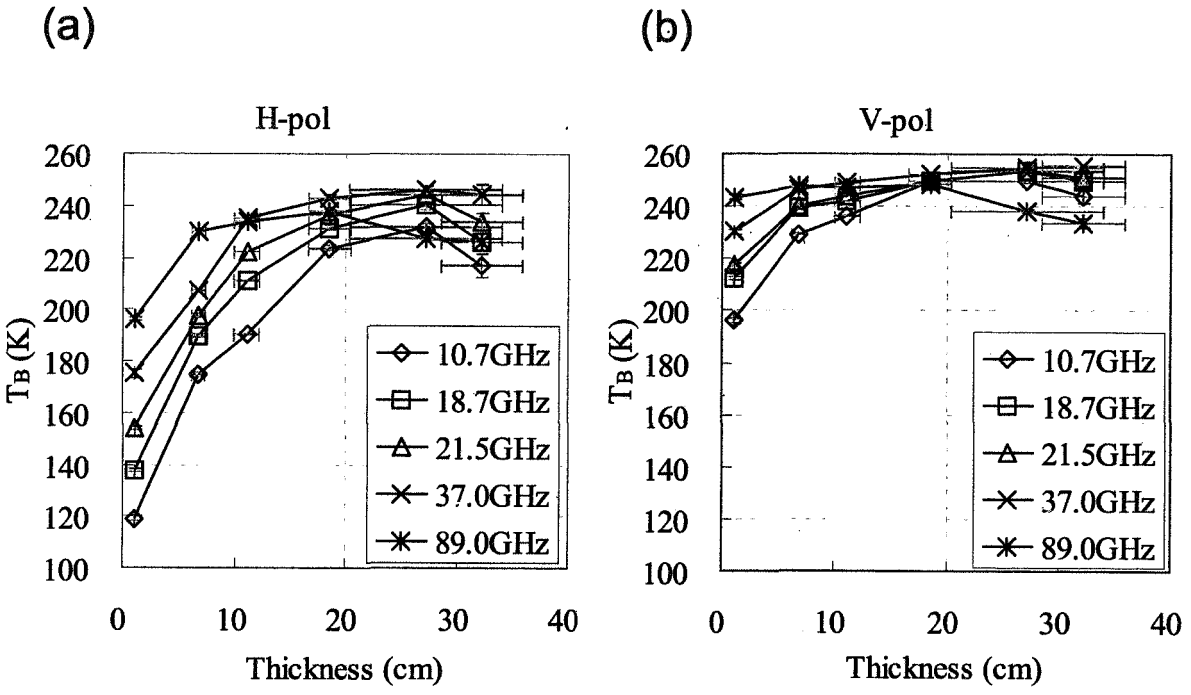
(a)
H-pol
260
240
220
200
180
160
140
120
100
T_B (K)
0
10
20
30
40
Thickness (cm)
10.7GHz
18.7GHz
21.5GHz
37.0GHz
89.0GHz
(b)
V-pol
260
240
220
200
180
160
140
120
100
T_B (K)
0
10
20
30
40
Thickness (cm)
10.7GHz
18.7GHz
21.5GHz
37.0GHz
89.0GHz

Figure 4

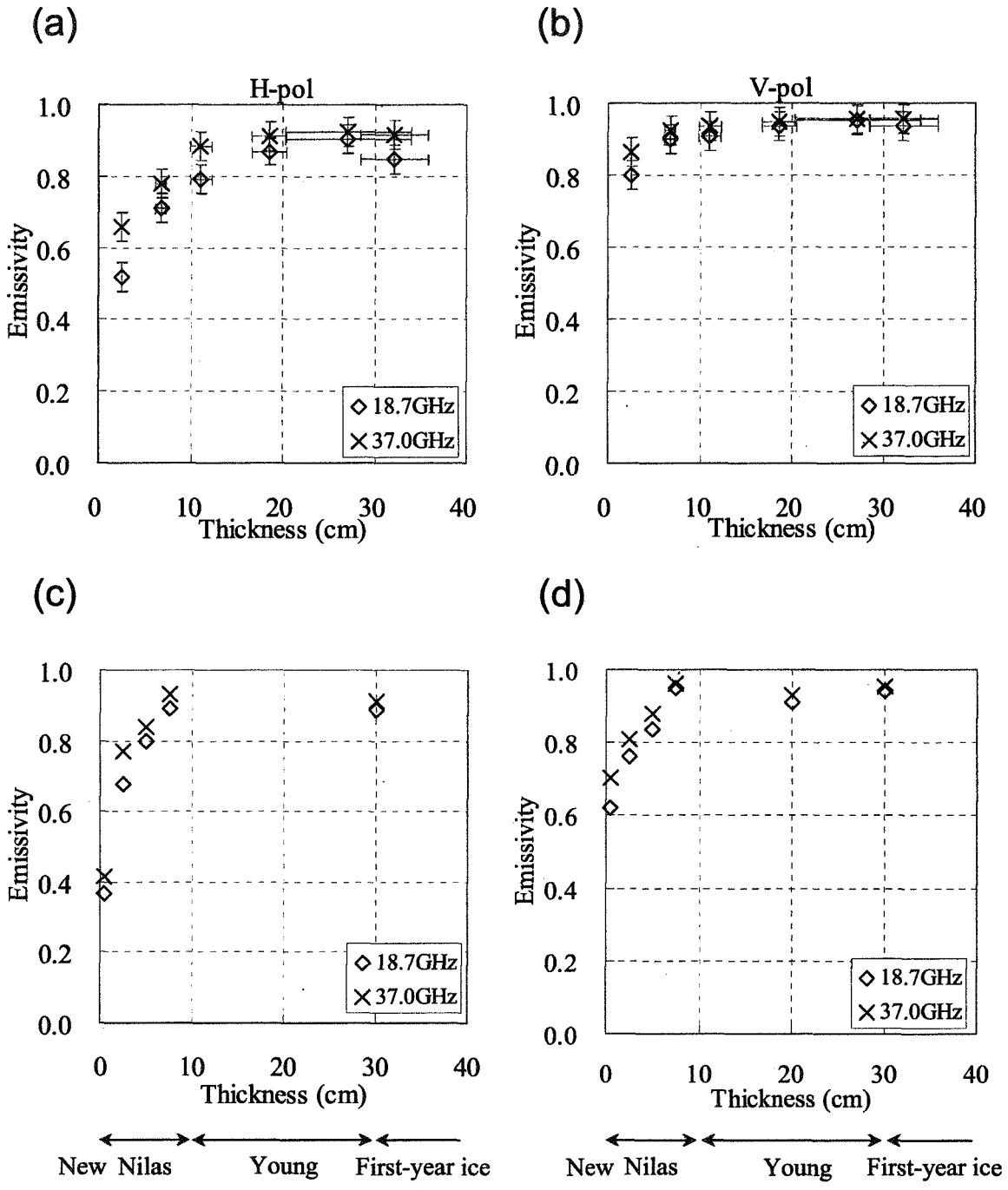
(a)
H-pol
Emissivity
Thickness (cm)
◇18.7GHz
×37.0GHz
(b)
V-pol
Emissivity
Thickness (cm)
◇18.7GHz
×37.0GHz
(c)
Emissivity
Thickness (cm)
◇18.7GHz
×37.0GHz
New Nilas
Young
First-year ice
(d)
Emissivity
Thickness (cm)
◇18.7GHz
×37.0GHz
New Nilas
Young
First-year ice

Figure 5

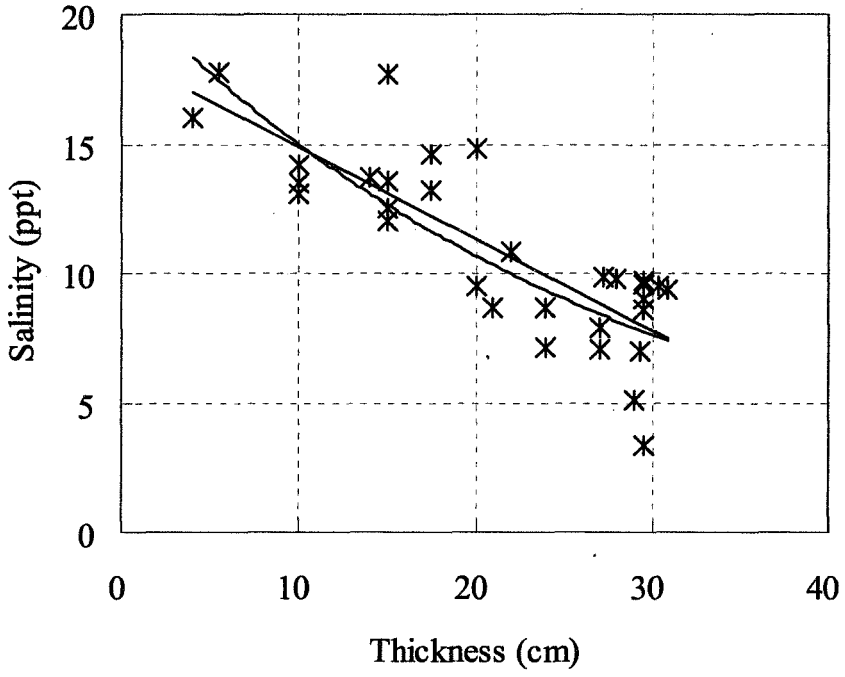

Figure 6

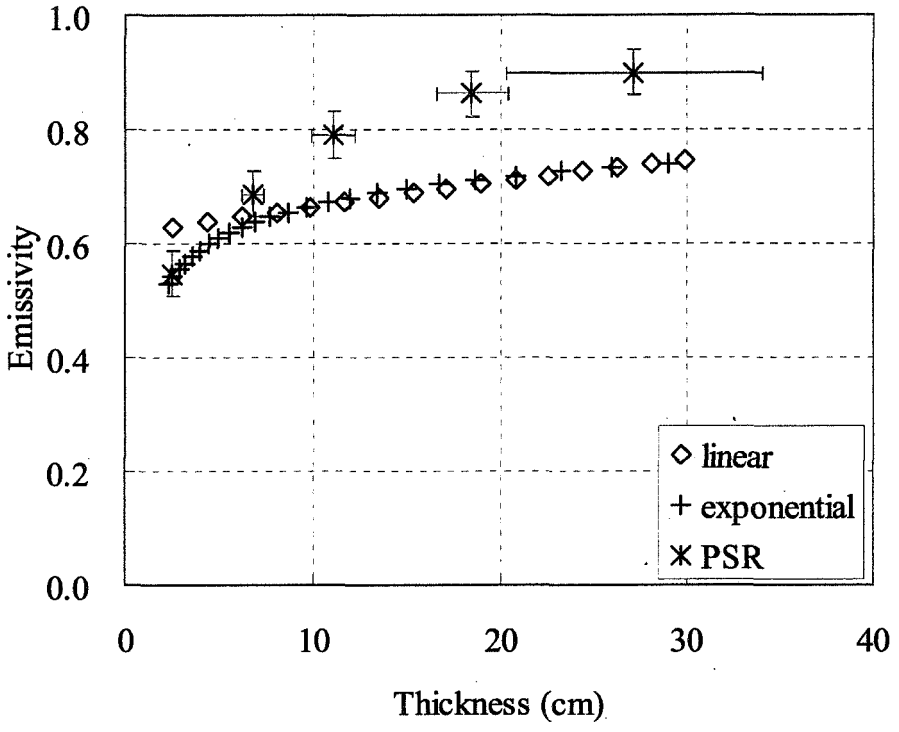
1.0
0.8
0.6
0.4
0.2
0.0
Emissivity
0
10
20
30
40
Thickness (cm)
linear
exponential
PSR

Figure 7

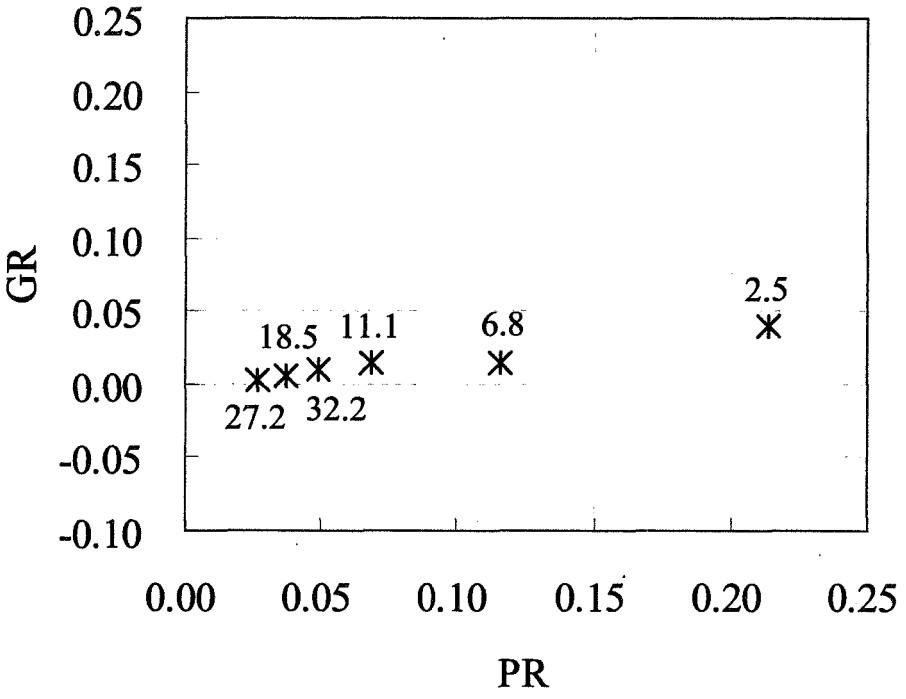
0.25
0.20
0.15
0.10
0.05
0.00
-0.05
-0.10
GR
0.00
0.05
0.10
0.15
0.20
0.25
PR
18.5
11.1
6.8
2.5
27.2
32.2

Figure 8

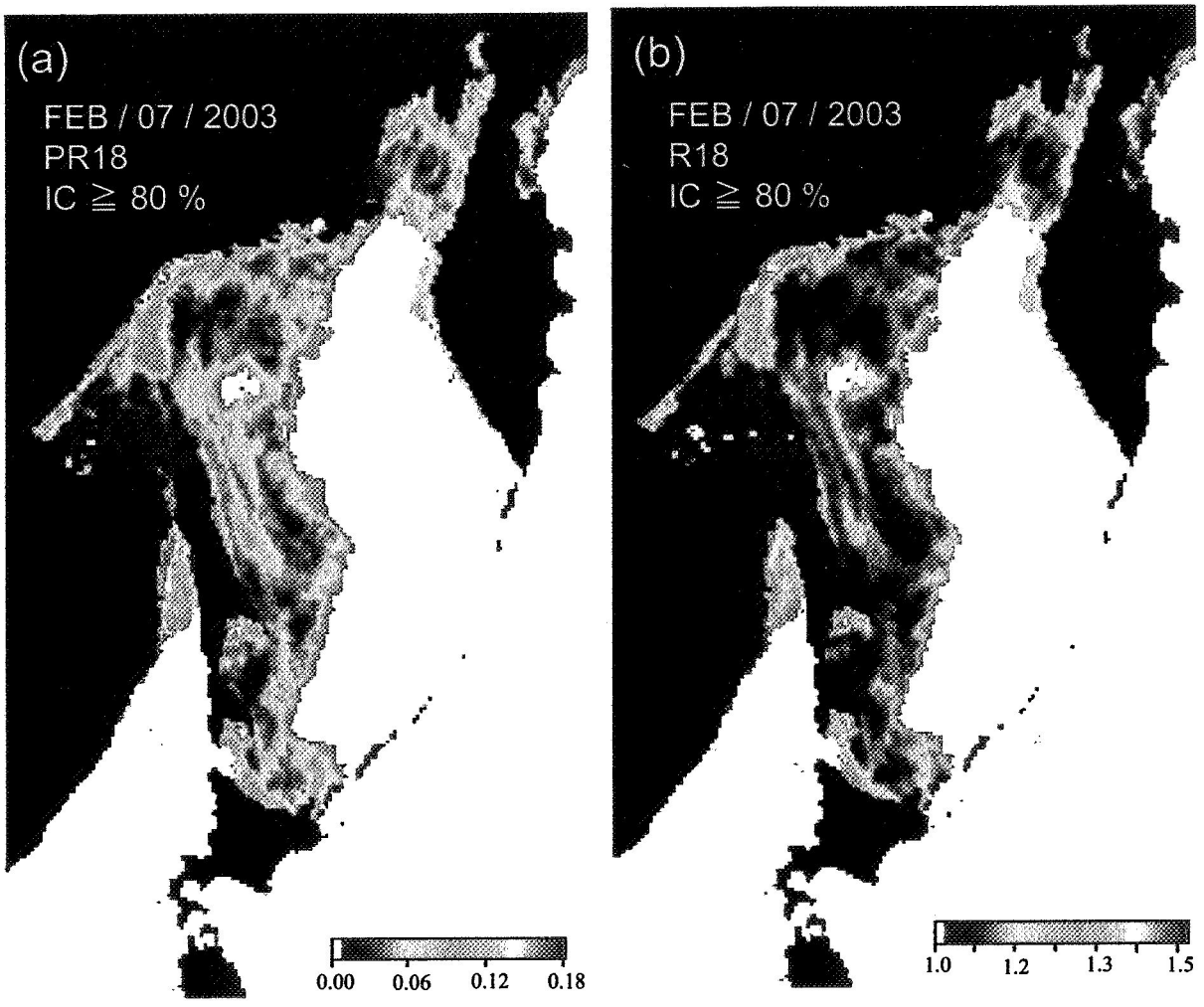
(a)
FEB / 07 / 2003
PR18
IC ≧ 80 %
0.00
0.06
0.12
0.18
(b)
FEB / 07 / 2003
R18
IC ≧ 80 %
1.0
1.2
1.3
1.5

Figure 9